JOURNAL OF GEOPHYSICAL RESEARCH, VOL. 112, B06306, doi:10.1029/2006JB004720, 2007

Source distribution of Earth's background free oscillations

K. Nishida[1] and Y. Fukao[2]

Received 28 August 2006; revised 12 January 2007; accepted 12 February 2007; published 21 June 2007.

[1] Recently a few groups reported existence of Earth's background free oscillations even on seismically quiet days. Observed features suggest that they are persistently excited on or just above the Earth's surface owing most likely to atmospheric and/or oceanic disturbances. To constrain their excitation mechanisms we developed a new method for estimation of spatial distribution of their excitation sources by modeling cross spectra between pairs of stations. The method is to calculate synthetic cross spectra for spatially homogeneous distribution of random sources and invert with them the observed cross spectra to the heterogeneous source distribution. We applied this method to the IRIS records at 54 stations during 1988–2000. The result showed clear temporal variations of spatial patterns. From November to April the spatial distribution shows a degree 1 pattern with the maximum in the North Pacific Ocean. From May to October strong excitation sources are located along the eastern and western Pacific rims through the Indian Ocean. In all the time periods, excitation sources on continents are weaker than in oceanic areas. This temporal variation of the spatial pattern is qualitatively consistent with that reported by Rhie and Romanowicz (2004). However, the excitation sources are not localized in shallow seas, as might be expected from the hypothesis of excitation by ocean infragravity waves, but must be distributed on the whole sea surface.

Citation: Nishida, K., and Y. Fukao (2007), Source distribution of Earth's background free oscillations, *J. Geophys. Res.*, *112*, B06306, doi:10.1029/2006JB004720.

1. Introduction

[2] It has long been believed that only large earthquakes excite free oscillations of the solid Earth. Recently, however, a few groups reported Earth's background free oscillations even on seismically quiet days [e.g., *Nawa et al.*, 1998; *Suda et al.*, 1998; *Kobayashi and Nishida*, 1998; *Tanimoto*, 1998]. The excited modes are almost exclusively fundamental spheroidal modes, and they fluctuate persistently in little correlation with their neighboring modes [*Nishida and Kobayashi*, 1999]. These features suggest that the background free oscillations are excited incessantly by random disturbances globally distributed near the Earth's surface [*Nishida and Kobayashi*, 1999]. The intensities of these modes clearly show annual and semiannual variations with the largest peak in July and a secondary peak in January [*Nishida et al.*, 2000; *Tanimoto*, 1999; *Ekström*, 2001]. The observed amplitudes of some modes are anomalously large relative to the adjacent modes [*Nishida et al.*, 2000]. These are the modes that are theoretically expected to be coupled with the acoustic modes of the atmospheric free oscillations [*Watada*, 1995]. All of these features suggest that atmospheric disturbance is one of the most likely excitation sources of this phenomenon [*Nishida and Kobayashi*, 1999; *Nishida et al.*, 2000].

[3] To constrain the excitation mechanism, *Rhie and Romanowicz* [2004] determined the locations of the excitation sources of these oscillations, using two arrays of broadband seismometers, one is in California and the other in Japan. Their results show that excitation sources are dominated on the north Pacific ocean in winter of the northern hemisphere and on the southern hemisphere near the South Pole in winter of the southern hemisphere. By comparing this result to the oceanic wave height data they concluded that the most probable excitation source is oceanic disturbance. Because they used a nonlinear stack method (phase weighted stack [i.e., *Rost and Thomas*, 2002]) for the records of only two arrays, the excitation source they determined can be a spatial average of globally distributed sources which depends on the source and array configurations and the source intensity distribution. The excitation sources are, in fact, likely to be globally distributed, as indicated by studies of mode-to-mode correlations [*Nishida and Kobayashi*, 1999] and station-to-station correlations [*Nishida et al.*, 2002] of the background free oscillations.

[4] In this study, we develop a method to obtain spatial information about the randomly distributed excitation sources over the globe and apply it to the real data. We first calculate the Earth response to persistently excited random sources homogeneously distributed over the globe, which is given as the synthetic cross spectrum between a pair of

[1]Earthquake Research Institute, University of Tokyo, Tokyo, Japan.
[2]Japan Agency for Marine-Earth Science and Technology, Kanagawa, Japan.

0148-0227/07/2006JB004720$09.00

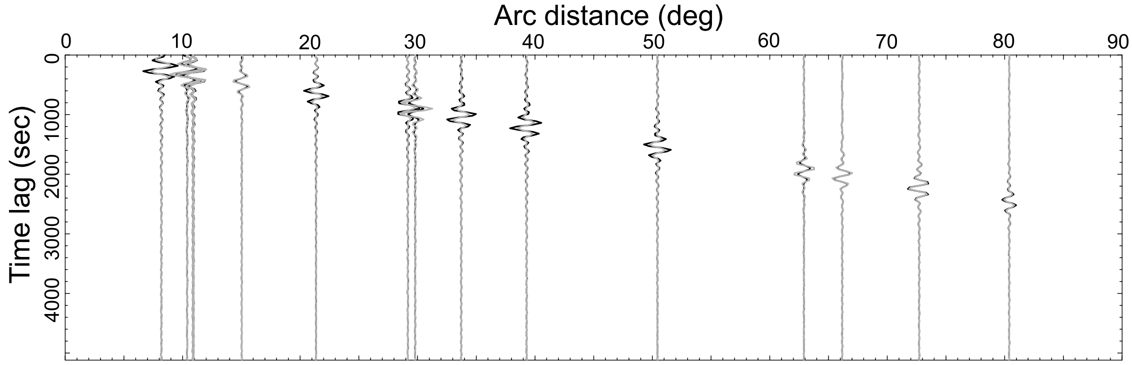

Figure 1. Typical examples of observed cross-correlation functions with good signal-to-noise ratios (gray) and the synthetic ones (black) calculated for spatially homogeneous sources, both of which are bandpass-filtered from 3 to 6 mHz.

stations. The observed cross spectra between all the station pairs are then inverted with the corresponding Earth responses to the spatially variable excitation sources. Inversion is made using records in every 2 months to see the possible temporal variation of the spatial characteristics of the excitation sources.

2. Data

[5] We analyze 10-s continuous sampling records in a time period from 1988 to 2000 through the very-long-period high-gain (VH) channel from the vertical STS-1 seismometers at 54 stations at the lowest ground noise levels of slightly less than 3×10^{-18} m^2 s^{-3}. The records are provided by the Incorporated Research Institutions for Seismology Data Management Center (IRIS DMC) [*IRIS, Inc.*, 1994]. For each station, we remove glitches and divide the whole record into about 5.6 hour segments with an overlap of 1 hour. Each of the segments is Fourier-transformed to obtain the power spectrum. The spectrum might have been disturbed by transient phenomena such as earthquakes and local nonstationary ground or instrumental noise. We discard all the seismically disturbed segments which are defined in terms of the mean power spectral densities (PSDs) greater than 3×10^{-18} m^2 s^{-3} in a frequency range 2.5–7.5 mHz. We also discard noisy segments if their mean PSDs over the four frequency ranges, 7.5–12.5, 12.5–17.5 and 17.5–22.5 mHz are greater than 3×10^{-18} m^2 s^{-3} [*Nishida and Kobayashi*, 1999]. We calculate the cross-correlation function and cross spectrum between every pair of different stations for their common record segments with sampling lengths of 2 months (60 days). Such calculations are made for each of the thirteen years. We then obtain yearly averages of the cross-correlation functions and cross spectra of the records 2 months long between every pair of two stations.

[6] If the fundamental Rayleigh waves are excited by homogeneous and isotropic sources as a stationary stochastic process, the display of the cross-correlation functions between two stations as a function of their separation distance should indicate clear Rayleigh wave propagation [*Nishida et al.*, 2002]. This is in fact the case of the observed records as shown in Figure 1, where the cross-correlation functions obtained are bandpass-filtered from 3 to 6 mHz. The corresponding synthetic cross-correlation functions can be calculated by the method as will be described in section 3, where homogeneous and isotropic sources are assumed. In Figure 1 the calculated cross-correlation functions are superposed to the observed ones. Although they are in general in very good agreement, we still observe some small discrepancy, which we attribute to the effect of the lateral heterogeneity of the source distribution.

[7] The cross-correlation function between two stations is strongly sensitive to excitation sources randomly distributed in close proximity of the great circle path where waves radiated from them interfere constructively while waves radiated from sources off the great circle path interfere destructively [*Snieder*, 2004] (see section 3 and Figure 3 therein for detail). Therefore, if there is any heterogeneity in the spatial distribution of excitation sources, the observed cross-correlation functions must be deviated from the synthetic cross-correlation functions calculated for the homogeneously distributed excitation sources, and the plot of these deviations at the poles of the station-to-station great circle paths must have some structure. We define the deviation r as $r = [A_{obs} - A_{syn}]/A_{syn}$ where A_{obs} and A_{syn} are the peak-to-trough amplitudes of the observed and synthetic cross-correlation functions. We calculate the r values for the six periods from January–February to November–December for every pair of two stations. In Figure 2 we plot these r values at the poles of their corresponding great circle paths. This figure shows clearly a degree two-dominant structure, demonstrating that the records carry information about the spatial distribution of excitation sources indeed.

3. Forward Problem: Synthetic Cross Spectra for Distributed Sources

[8] We assume that the Earth's background free oscillations are excited by spatially isotropic but heterogeneous dynamic pressure disturbances at the Earth's surface. Following *Fukao et al.* [2002] we calculate a synthetic cross spectrum between a station at $\mathbf{x}_1$ and that at $\mathbf{x}_2$ by summing fundamental spheroidal modes, which are confirmed to be the dominant modes by many observations [e.g., *Suda et al.*,

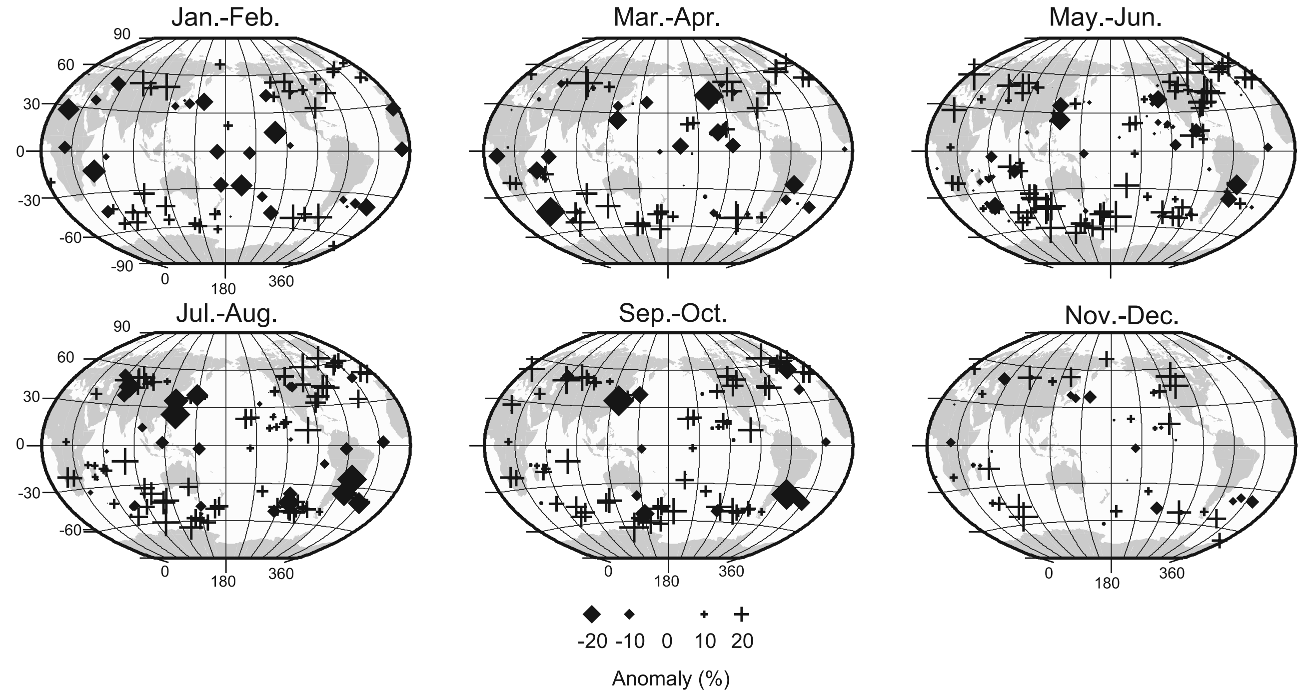

Figure 2. Amplitude anomalies of cross-correlation functions plotted at the poles of the great circle paths between pairs of stations in January. Crosses and diamonds indicate positive and negative anomalies, respectively.

1998; *Kobayashi and Nishida*, 1998]. The Cross spectrum of ground acceleration Φ can be expressed as

$$\Phi(\mathbf{x}_1, \mathbf{x}_2; \omega) = \sum_{ll'} \frac{\eta_l(\omega)\eta^*_{l'}(\omega)}{4\pi^2 R^2} \sum_{mm'} \mathcal{Y}_{lm}(\theta_1, \phi_1)\mathcal{Y}_{l'm'}(\theta_2, \phi_2) \int_\Sigma d\Sigma' \int_\Sigma d\Sigma'' \Psi(\mathbf{x}', \mathbf{x}''; \omega)\mathcal{Y}_{lm}(\theta', \phi')\mathcal{Y}_{l'm'}(\theta'', \phi''), \tag{1}$$

where $\Psi(\mathbf{x}', \mathbf{x}''; \omega)$ between $\mathbf{x}'$ and $\mathbf{x}''$ is cross-spectral density of pressure disturbance at Earth's surface Σ. Here η_l is a resonance function of the l'th mode defined as

$$\eta_l(\omega) = \frac{2\pi R U_l^2(R)\omega^2}{\left[-\frac{\omega_l}{2Q_l} - i(\omega_l - \omega)\right]\left[-\frac{\omega_l}{2Q_l} + i(\omega_l + \omega)\right]}, \tag{2}$$

where R is the Earth's radius, ω_l is eigen-frequency of the l'th fundamental spheroidal mode and Q_l is quality factor of the l'th mode, vertical eigen function of the l'th mode U_l and surface spherical harmonics $\mathcal{Y}_{lm}(\theta_1, \phi_1)$ are defined as in work of *Dahlen and Tromp* [1998].

[9] We assume that cross-spectral density of pressure disturbance $\Psi(\mathbf{x}', \mathbf{x}''; \omega)$ between $\mathbf{x}'$ and $\mathbf{x}''$ can be represented as

$$\Psi(\mathbf{x}', \mathbf{x}''; \omega) = \sqrt{\hat{\Psi}(\mathbf{x}'; \omega)\hat{\Psi}(\mathbf{x}''; \omega)}\, h\left(\frac{|\mathbf{x}' - \mathbf{x}''|}{\sqrt{L(\mathbf{x}', \omega)L(\mathbf{x}'', \omega)}}\right), \tag{3}$$

where $\hat{\Psi}(\mathbf{x}; \omega)$ is the PSD of pressure disturbance, $L(\mathbf{x}', \omega)$ is the frequency-dependent coherence length. Function $h(x)$ is 1 when $0 \leq x \leq 1$ and 0 otherwise. Coherence length L has been reported to be less than 1 km in the mHz band [*Fukao et al.*, 2002] and is anyway much shorter than the wavelengths of fundamental spheroidal modes, which are on the order of 1000 km. This situation makes it possible to express $\Phi(\mathbf{x}_1, \mathbf{x}_2; \omega)$ using Green function $G(\mathbf{x}_1, \mathbf{x}_2; \mathbf{x}, \omega)$ and source function $\hat{\Psi}_e(\mathbf{x}, \omega)$ where G and $\hat{\Psi}_e$ are viewed as functions of $\mathbf{x}$,

$$\Phi(\mathbf{x}_1, \mathbf{x}_2; \omega) = \int_\Sigma d\Sigma G(\mathbf{x}_1, \mathbf{x}_2; \mathbf{x}, \omega)\hat{\Psi}_e(\mathbf{x}, \omega). \tag{4}$$

Source function $\hat{\Psi}_e$ is the power spectrum of effective pressure at $\mathbf{x}$ given by

$$\hat{\Psi}_e(\mathbf{x}, \omega) \equiv \frac{L^2(\mathbf{x}, \omega)}{4\pi R^2}\hat{\Psi}(\mathbf{x}, \omega). \tag{5}$$

It is this effective pressure $\hat{\Psi}_e$, rather than pressure itself $\hat{\Psi}$, that contributes to Φ. Green function G represents the Earth response to unit effective pressure acting at $\mathbf{x}$, which is given by

$$G(\mathbf{x}_1, \mathbf{x}_2; \mathbf{x}, \omega) = \sum_{ll'} \eta_l(\omega)\eta^*_{l'}(\omega) \sum_{mm'} \mathcal{Y}_{lm}(\theta_1, \phi_1)\mathcal{Y}_{l'm'}(\theta_2, \phi_2)\mathcal{Y}_{lm}(\theta, \phi)\mathcal{Y}_{l'm'}(\theta, \phi). \tag{6}$$

[10] To make calculation of cross-spectral density Φ feasibly (equation (4)), we expand the Green function G and source function $\hat{\Psi}_e$ by spherical harmonics up to degree l_0. We expand $\hat{\Psi}_e$ by assuming that $\hat{\Psi}_e$ can be separated into the

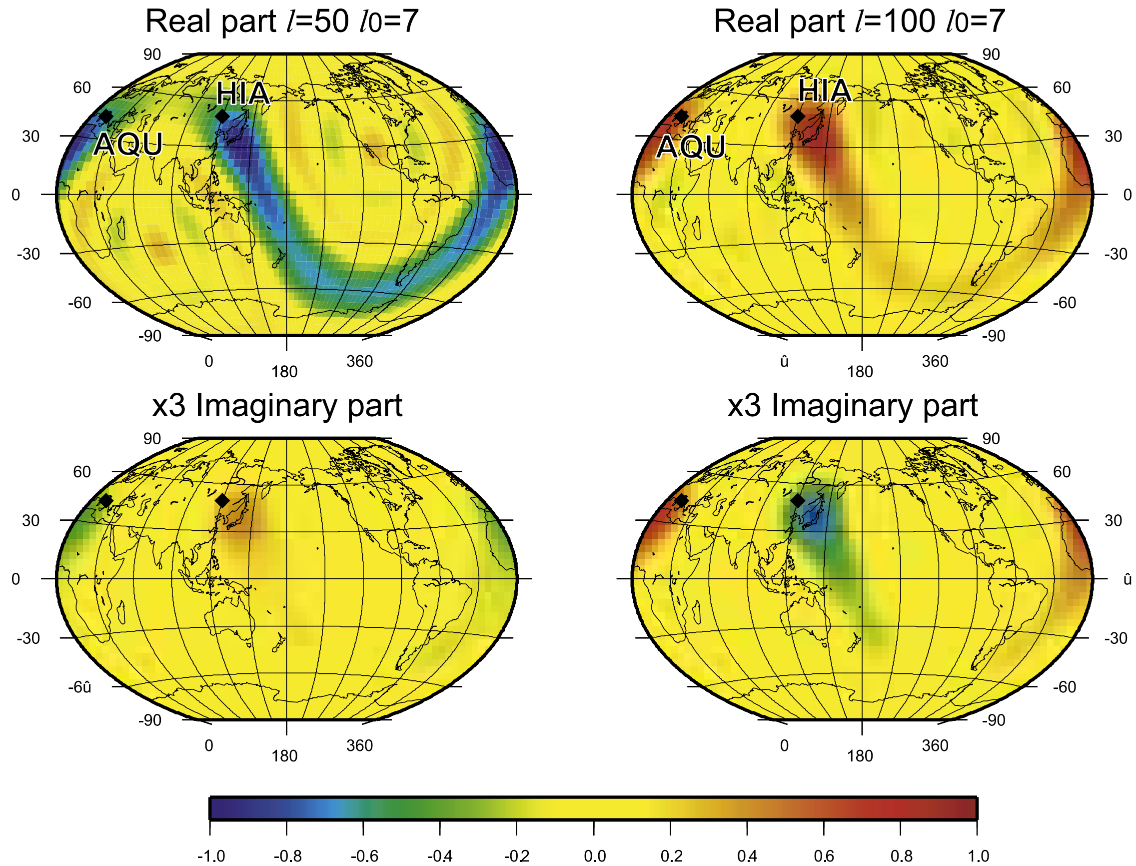

Figure 3. Green function of cross spectrum between AQU and HIA (left) at about 5.6 mHz corresponding to the eigen-frequency of ${}_0S_{50}$ and (right) at about 10 mHz corresponding to ${}_0S_{100}$. The cutoff angular order l_0 is set at 7. The real part of the Green Function (top plots) is normalized by its maximum value. The imaginary part (bottom plots) is normalized by the one third of the maximum value of the real part. Both the real and imaginary parts have sensitivities along the great circle path with greater sensitivities along the major arc.

spatial and frequency parts. The expansion is truncated at angular degree l_0 to obtain a truncated source function,

$$\hat{\Psi}_e^{l_0}(\mathbf{x};\omega) \equiv \Psi_e^0(\omega)\sum_l^{l_0}\sum_m c_{lm}\mathcal{Y}_{lm}(\theta,\phi). \quad (7)$$

We also expand G by spherical harmonics up to degree l_0 to obtain a truncated Green function,

$$G^{l_0}(\mathbf{x}_1,\mathbf{x}_2;\mathbf{x},\omega) \equiv \sum_l^{l_0}\sum_m \mathcal{Y}_{lm}\hat{G}_{l,m}. \quad (8)$$

Here $\hat{G}_{l,m}$ is the coefficient of spherical harmonic expansion defined by

$$\hat{G}_{l,m}(\mathbf{x}_1,\mathbf{x}_2;\omega) = R^2\sum_{l'l''}\eta_{l'}(\omega)\eta_{l''}^*(\omega)\sum_{m'm''}\mathcal{Y}_{l'm'}(\theta_1,\phi_1)\mathcal{Y}_{l''m''}(\theta_2,\phi_2)$$
$$\int_\Sigma \mathcal{Y}_{lm}(\theta,\phi)\mathcal{Y}_{l'm'}(\theta,\phi)\mathcal{Y}_{l''m''}(\theta,\phi)d\sigma, \quad (9)$$

where σ represents the surface of unit sphere.

[11] We now approximate cross-spectral density Φ by using the spatially truncated source function and the spatially truncated Green function,

$$\Phi^{l_0}(\mathbf{x}_1,\mathbf{x}_2;\omega) = \int_\Sigma \hat{\Psi}_e^{l_0}(\mathbf{x};\omega)G^{l_0}(\mathbf{x}_1,\mathbf{x}_2;\mathbf{x},\omega)d\Sigma. \quad (10)$$

[12] Figure 3 shows the truncated Green functions for a station-pair of AQU and HIA at frequencies of about 5.6 and 10 mHz corresponding to the eigen-frequencies of ${}_0S_{50}$ and ${}_0S_{100}$, respectively. The cutoff angular order l_0 is set at 7. The Green function at a given frequency has a sensitivity mainly along the major arc of the great circle connecting two stations, provided that their separation, $|\mathbf{x}_1 - \mathbf{x}_2|$, is longer than the wavelengths of spheroidal modes in the vicinity of that frequency. The real part shows a symmetric pattern on the great circle with respect to the midpoint of the two stations, while the imaginary part shows an antisymmetric pattern. The analogy can be found in description of scattering of ballistic waves [*Snieder*, 2004]. The above properties of the truncated Green function G^{l_0} may also be understood by its spherical harmonic expansion equation (8), where coefficients $\hat{G}_{lm}$ with even l contribute more to G^{l_0}

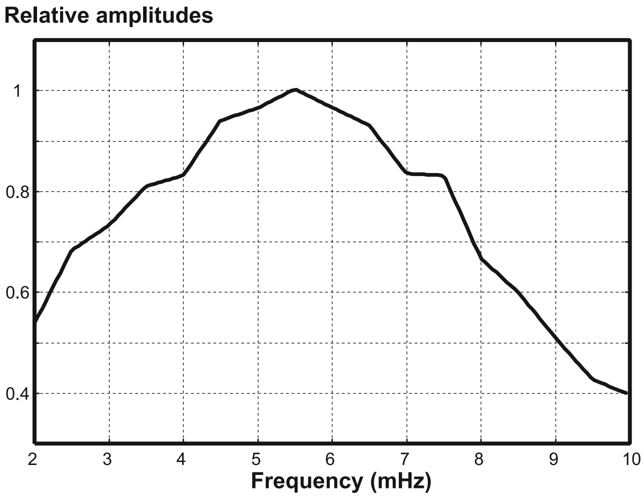

Figure 4. Estimated source spectrum of effective pressure in a period from January to February. Only the factor relative to the Fukao model (equation (13)) is shown.

than coefficients $\hat{G}_{lm}$ with odd l. Functions $\hat{G}_{lm}$ with odd l contribute mainly to the imaginary part of G^{l_0} through mutual overlapping of resonant functions with different angular orders because of their broadening due to attenuation (see equation (6)). The imaginary part of the Green function increases its amplitude with frequency relative to the real part. Using the modes at high frequencies, therefore, we could determine in principle the odd-degree structure, although its accuracy is likely to be degraded as compared to the even-degree structure.

[13] We have so far developed a forward scheme; given a spatial distribution of effective pressure sources, the excitation of Earth's free oscillations be calculated. We now develop the inverse scheme: knowing the Earth response to random excitation sources, their spatial distribution be estimated. For this purpose we rewrite cross-spectrum Φ^{l_0} as

$$\Phi^{l_0}(\mathbf{x}_1, \mathbf{x}_2; \omega) = \Psi_e^0(\omega) \sum_l \sum_m c_{lm} \hat{G}_{l,m}(\mathbf{x}_1, \mathbf{x}_2; \omega). \tag{11}$$

4. Two-Step Inversion

[14] We infer the spatial structure of effective pressure sources through two steps. The first step is to extract the most dominant component of the spatial distribution of effective pressure sources, which is in this case the spatially homogeneous component (l = 0) as is obvious from Figure 1. This component is so dominant that it can be used as the reference model of the source distribution. The next step is to extract the higher angular order components ($l = 1 - 7$) by inverting the observed cross spectra.

4.1. First Step: Construction of Reference Homogeneous Source Model

[15] We first obtain the reference model of effective pressure $\Psi_e^0(\omega)$ in every interval of 2 months, assuming that the spatial part of excitation sources is homogeneous, a reasonable assumption as demonstrated in Figure 1. For this reference model we can simplify the synthetic cross-spectrum $\hat{\Phi}^0$ between the i'th and j'th stations as

$$\hat{\Phi}^0(\mathbf{x}_i, \mathbf{x}_j; \omega) = \Psi_e^0(\omega) R^2 \sum_l \frac{2l+1}{4\pi} \eta_l^2(\omega) P_l(\cos(\Theta_{ij})), \tag{12}$$

where Θ_{ij} is the angle between $\mathbf{x}_i$ and $\mathbf{x}_j$. To obtain an expression for Ψ_e^0, we start with the empirical model of *Fukao et al.* [2002], which is expressed as

$$\Psi_e^{in}(f) = \frac{2 \times 10^9}{4\pi R^2} \left(\frac{f}{f_0}\right)^{-2.3}, \tag{13}$$

where f_0 is 1 mHz. This model explains the observed background free oscillation modes at frequencies below 6 mHz, which will be modified so that it can explain the higher-frequency modes as well. The expression of Ψ_e^0 is obtained by multiplying a series of triangular functions to Ψ_e^{in},

$$\Psi_e^0(\omega) = \Psi_e^{in}(\omega) \sum_{i=4}^{21} a_i B_i(\omega), \tag{14}$$

where $B_i(\omega)$ is a triangular function defined as

$$B_i(\omega) = \begin{cases} \frac{\omega - \omega_0(i-1)}{\omega_0} & \omega_0(i-1) < \omega \le \omega_0 i \\ -\frac{\omega - \omega_0(i+1)}{\omega_0} & \omega_0 i \le \omega \le \omega_0(i+1) \\ 0 & \text{otherwise,} \end{cases} \tag{15}$$

with the reference angular frequency ω_0 at 5×10^{-4} Hz. Because the observed cross-spectrum $\Phi(\mathbf{x}_1, \mathbf{x}_2; \omega)$ is the one for the tapered records, we must take into account the effect of tapering in the synthetic cross-spectrum $\hat{\Phi}^0(\mathbf{x}_i, \mathbf{x}_j; \omega)$. The expression including this effect is given by convolution of $\hat{\Phi}^0$ with the PSD of the taper function, $\Gamma(\omega)$.

[16] We determine the coefficients a_i in equation (14) by minimizing the squared difference S between the observed and synthetic cross spectra, which is defined as

$$S = \sum_{i=1}^{N} \sum_{j=1}^{i-1} \sum_{k=0}^{M} \left(\Phi_{ij}^{ob}(\omega_k) - \frac{\Phi^0(\mathbf{x}_i, \mathbf{x}_j; \omega_k) * \Gamma(\omega_k)}{2\pi} \right)^2, \tag{16}$$

where N is the number of stations, Φ_{ij}^{ob} is an observed cross spectrum, * denotes convolution and ω_k ($k = 0, \cdots, K-1$) is the observed frequency from 2 to 10 mHz. In the summation we use only the cross-spectral terms ($i \neq j$) and exclude the power-spectral terms ($i = j$) to avoid effects of self and local noises of seismometers. We determine a_i to minimize S as $\partial S / \partial a_i = 0$.

[17] Figure 4 shows an example of the reference source spectrum of effective pressure $\hat{\Phi}_e^0$, where only the factor $\sum_{i=4}^{21} a_i B_i$, rather than the whole term $\Psi_e^{in} \sum_{i=4}^{21} a_i B_i$, is shown. The sampling time in this example is 2 months from January to February, stacked from all the years. At about 5.5 mHz the factor takes its maximum value of approximately 1, indicating that Ψ_e^{in} best approximates the effective pressure $\hat{\Phi}_e^0$ around this frequency, below and above which it tends to exceed $\hat{\Phi}_e^0$.

4.2. Second Step: Inversion for Spatial Distribution

[18] We next infer the spatial distribution of effective pressure sources relative to the reference homogeneous

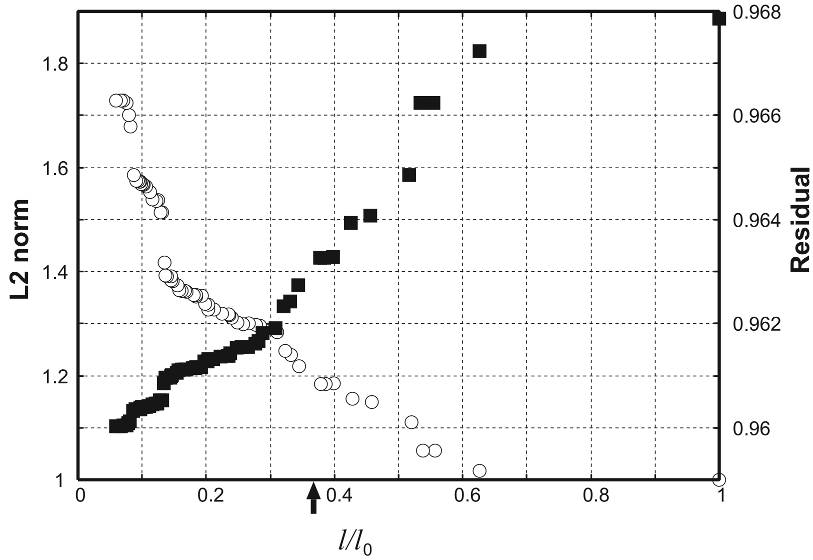

Figure 5. Tradeoff curves against singular value λ normalized by its maximum value λ_0. Prediction error (open circle) is defined by the sum of the squared difference between the observed data and the prediction from the model, normalized by the sum of the squared data. Model parameter length (solid square) is defined by the L2 norm of the estimated model parameters. Arrow shows the truncation of the normalized singular values at 0.36.

source model, assuming that the spatial pattern is frequency-independent in a frequency range from 2 to 10 mHz. We write the observation equations as $\mathbf{Ab} = \mathbf{d}$, where complex matrix $\mathbf{A}$, real model vector $\mathbf{m}$ and complex data vector $\mathbf{d}$ are defined as

$$A_{pq} \equiv w_{ij} \frac{\hat{G}_{lm}(\omega_k) * \Gamma(\omega_k)}{2\pi\sqrt{l^2 + s^2}} \tag{17}$$

$$d_q \equiv w_{ij}\left(\Phi^{ob}(\omega_k) - \Phi^0(\omega_k)\right) \tag{18}$$

$$m_p \equiv \sqrt{l^2 + s^2} c_{lm}. \tag{19}$$

Here $p = l^2 + l + m + 1$, $q = (Nj + i)K + k$, s is a damping factor and w_{ij} is a data quality–dependent weight to the observed cross spectrum between the i'th and j'th stations. Note that the data to be inverted are not the observed cross spectra themselves but their residuals from the synthetic cross spectra calculated for the reference model so that the model parameters to be determined are the source heterogeneity components relative to the reference homogeneous source distribution. We find a value of 5 to be appropriate for the damping parameter s after some trial and errors.

[19] We estimate model parameter $\mathbf{m_{est}}$ using the SVD algorithm as

$$\mathbf{m_{est}} = \mathbf{A}^{-g}(\mathbf{d}), \tag{20}$$

where $\mathbf{A^{-g}}$ is the generalized inverse matrix: $\mathbf{A^{-g}} = \mathbf{V\Lambda_\lambda^{-1}U^T}$. Here we decompose $\mathbf{A}$ into

$$\mathbf{A} = \mathbf{U\Lambda V}^T, \tag{21}$$

where $\mathbf{U}$ and $\mathbf{V}$ are the orthogonal matrices, Λ is the diagonal matrix with singular values, ($\lambda_0 \geq \lambda_1 \geq, \ldots \geq \lambda_{(l_0+1)2}$), and Λ_λ^{-1} is the diagonal matrix with such elements as: $\Lambda_\lambda^{-1} = (1/\lambda_0, 1/\lambda_1, \ldots, 1/\lambda, 0, \ldots, 0)$.

[20] Figure 5 shows a trade-off between the prediction error (open circle) and the L^2 norm of model parameters $\Sigma c_{lm}^2/4\pi$ (solid square) as a function of λ_i/λ_0. The prediction error decreases while the model parameter length increases as λ_i/λ_0 increases. Both the plots of prediction error and model parameter length show locally flat portions at a singular value of about $\lambda_i = 0.36\lambda_0$, which is taken as the upper limit for the singular values to be used.

[21] Figure 6 shows the resolution matrix defined by $\mathbf{A^{-g}A}$, demonstrating that the degree 0, 1 and 2 structures are well resolved. Structures with even degrees 4 and 6 are resolved to some extent but those with odd degrees 3, 5 and 7 are not. As implied in Figure 6 and as confirmed directly by experiment, the resultant structure depends little on the cutoff angular order when it is higher than 7. The odd degree structures are poorly resolved except for degree 1 in part because their effect appears through relatively weak overlapping of resonant functions among different modes due to attenuation. The overlapping increases, in general, with increasing frequency. In Figure 3, for example, the Green function at 5.6 mHz is dominated by its real part which is symmetric with respect to the midpoint of the two stations, while the Green function at 10 mHz is contributed significantly from the imaginary part which is antisymmetric with respect to the midpoint of the two stations. Our inversion utilizes data from 2 to 10 mHz so that the 3rd and 5th degree structures could be resolved in principle. There is, however, another difficulty of retrieving these odd degree structures. This difficulty arises from a poorer station coverage in the Southern Hemisphere than in the Northern Hemisphere, resulting in a less spatial resolution of the Southern Hemisphere. A dense distribution of stations in

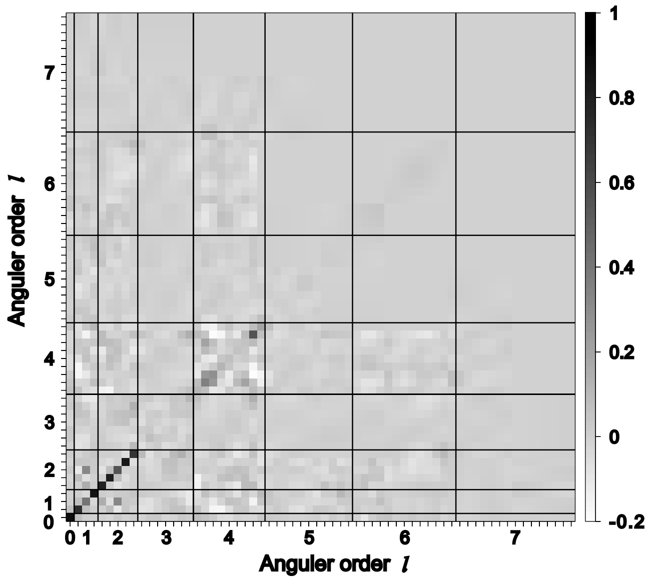

Figure 6. Resolution matrix $\mathbf{A}^{-g}\mathbf{A}$. Numbers attached to the vertical and horizontal axes are angular orders of the spherical harmonic expansion of source heterogeneity. Small tics along the axes indicate azimuthal orders associated with each angular order.

midlatitudes of the Northern Hemisphere contributes to relatively large diagonal components of the resolution matrix at l = 4 and m = ±3.

[22] The resolution matrix is somewhat difficult to capture spatial information of resolution. To estimate spatial resolution we make recovery tests for the localized trial models. The synthetic cross spectra are calculated for the source delta functions (Figure 7) truncated by angular degree 7 and are inverted by the method described above. We locate such trial models with their peak positions at latitudes 0, ±45° and longitudes 0, ±60, ±120, ±180°.

[23] Figure 8 shows the results of the recovery tests. Most of the figures show 10–20% recovery in amplitude due to damping applied in the inversion. Localized sources in the Northern Hemisphere are in general better recovered than those in the southern hemisphere because of the denser distribution of stations. The recovered image is in general broadened relative to the input but its peak position remains near the input position except for two cases corresponding to the peaks at 0°E 45°S and 60°W, 0°N. All of the figures show that our inversion can resolve a large-scale (~5000 km) structure of excitation sources, although there is some signal leakage to the antipode due in part to the lack of odd degree structures.

5. Spatial Distribution of Excitation Sources

[24] The solution $\mathbf{m}_{\mathbf{est}}$ is incorporated into equation (7) to obtain a spatial distribution of effective pressure. Figure 9 shows the result, $\hat{\Psi}_e^{l0}(\mathbf{x})/\Psi_e^0$, indicating clearly a temporal variation of the spatial pattern. During the period from November to April the degree 1 pattern with its maximum intensity in the northern Pacific is dominant. In the period from May to August the degree 1 pattern is diminished, and excitation sources are located on the eastern and western Pacific rims through the Indian Ocean. Sources in the southern hemisphere are active especially in a period from July to August. Resolution tests (Figure 8) show that we can roughly resolve source locations even in the southern hemisphere. The interval from September to October is a transitional stage between the above two periods. Through the year excitation sources are broadly located on oceans. Sources on continents are always weak.

[25] One may argue that our result obtained by a cross-correlation method might have been biased by lateral heterogeneity of seismic velocity structure. *Shapiro et al.* [2005] made a cross-correlation analysis of long sequences of ambient seismic noise around 0.1 Hz to obtain group velocity anomaly of Rayleigh waves due to lateral heterogeneity of the crust. The possible bias due to lateral heterogeneity is, however, expected to be small in the mHz band, where the perturbations of group velocity of Rayleigh waves are much smaller than those around 0.1 Hz. In fact, the source distribution pattern we obtained has little correlation with the well-known pattern of Rayleigh wave group velocity anomaly [e.g., *Larson and Ekström*, 2001] and changes from season to season, a feature not expected if the pattern is spuriously created by the lateral heterogeneity of the mantle. The effect of lateral heterogeneity may become serious if one wishes to use higher-frequency data above 10 mHz to obtain a finer source distribution.

[26] This temporal variation of the spatial pattern we obtained is qualitatively consistent with that reported by *Rhie and Romanowicz* [2004]. We, however, emphasize that excitation sources are not concentrated in narrow regions but are distributed semiglobally. We examine this point more quantitatively. Figure 10 shows the distribution of the power of relative effective pressure, $\Sigma_m c_{lm}^2/4\pi$, against spherical harmonic degree l. Clearly the source distribution is dominated by the 0'th degree structure. The 1'st degree structure shows a strong annual variation and its average power is at the same level as that of the 2'nd degree structure which shows little annual variation. Moving localized sources like typhoon could contribute to the 0'th degree dominance if they on the whole cover a very large area of the Earth's surface within every time window of

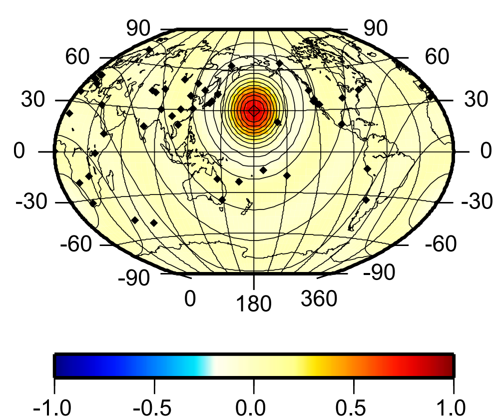

Figure 7. A truncated delta function with its peak value of 1 at 180°E 30°N. We made recovery tests using the synthetic data calculated for this type of input models. Diamonds indicate station location.

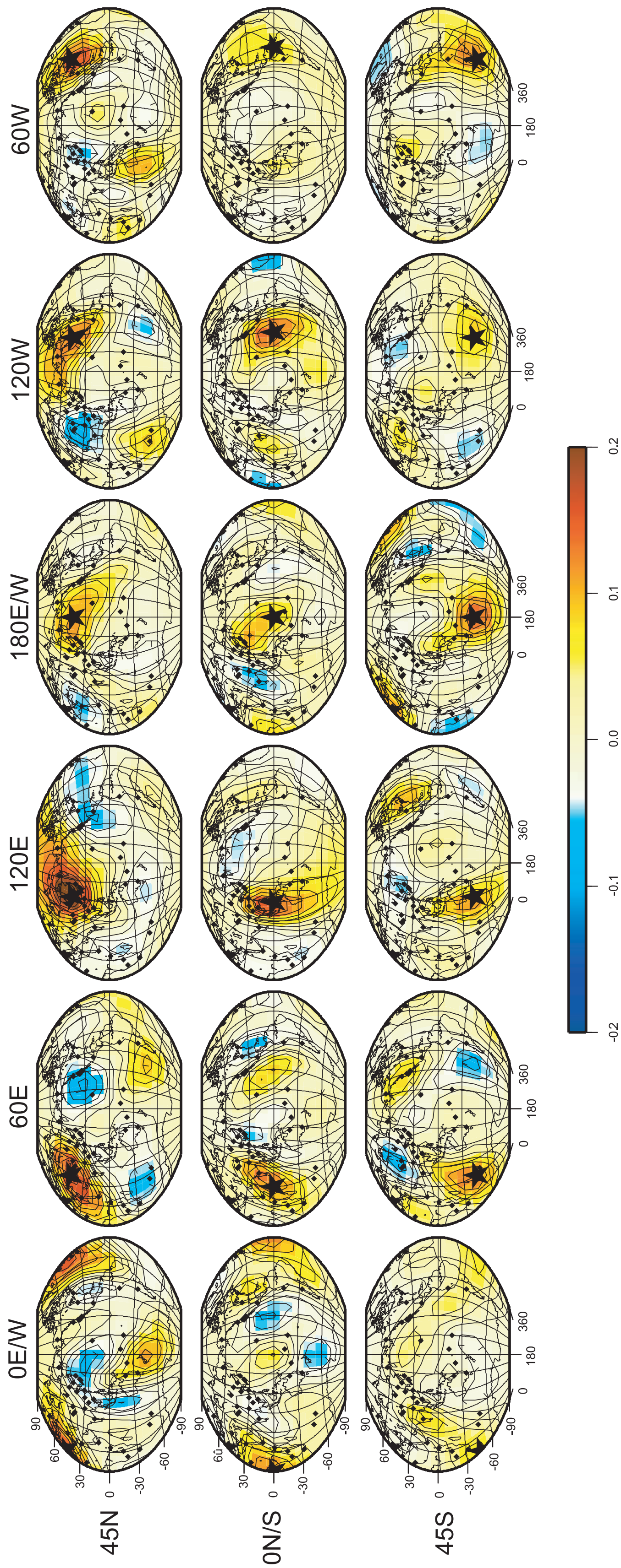

Figure 8. Results of the recovery tests for trial source models such as shown in Figure 7. A star in a map represents the source location of each of the trial models at latitudes 0°, ±45°, and longitudes 0°, ±60°, ±120°, 180°.

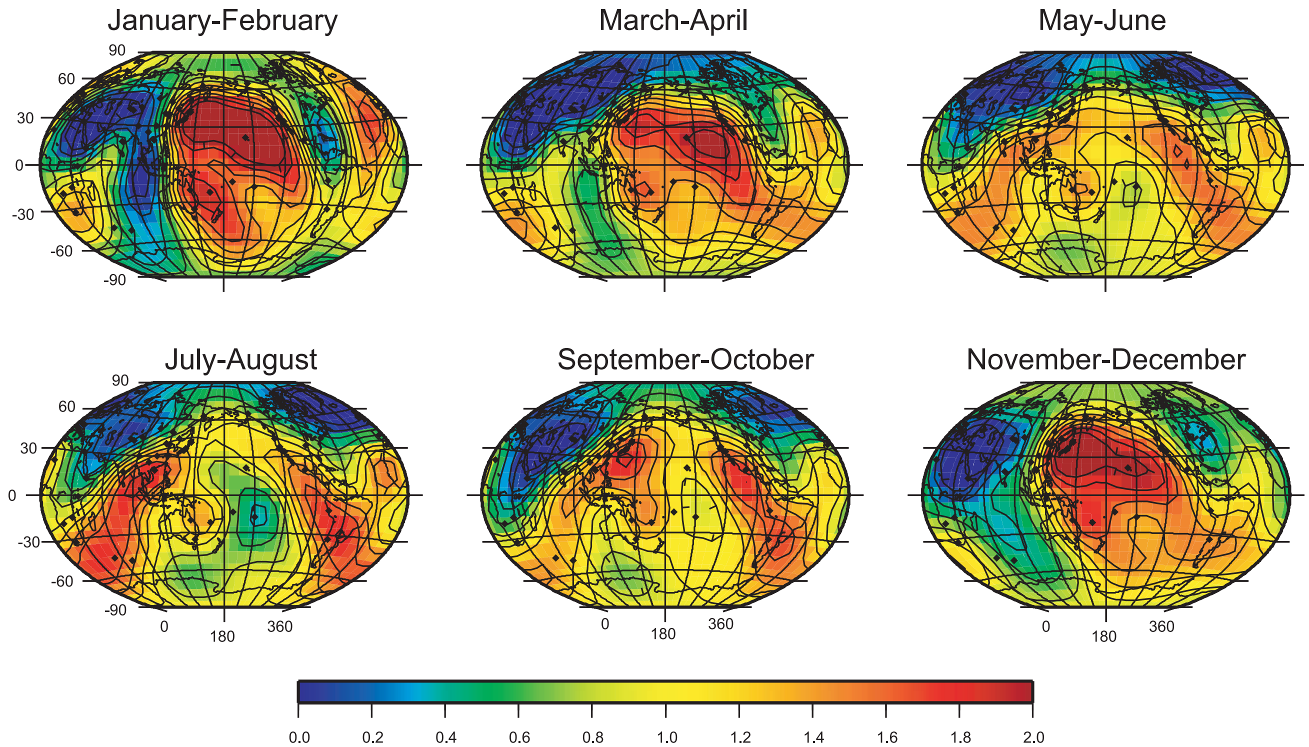

Figure 9. Spatial distribution of excitation sources estimated for every 2 months of a year. Indicated in color scale are relative amplitudes to the reference effective pressure model, $\hat{\Psi}_e^{l0}(\mathbf{x})/\Psi_e^0$.

2 months. This is a rather unlikely situation. It would also be difficult for such a moving source alone to explain the absence of the statistical correlation between the modes of the background free oscillations [*Nishida and Kobayashi*, 1999]. Our results strongly indicate that the excitation sources of the Earth's background free oscillations are not localized but spread over the almost whole oceanic areas, though we cannot determine from the present analysis whether they are within the atmosphere or oceans.

6. Discussion

[27] We discuss the results obtained above in relation to the two hypotheses for the excitation mechanisms. One is excitation by oceanic infragravity waves through the seafloor and the other is excitation by atmospheric disturbances through the sea surface and to less extent through the continental land surface.

[28] Pressure changes at the ocean bottom are dominated by that due to ocean swell in a frequency range from 5 to 50 mHz. This is one of the probable excitation sources of background free oscillations [*Watada and Masters*, 2001; *Rhie and Romanowicz*, 2004; *Tanimoto*, 2005]. Ocean swells in this frequency band are gravity waves often called infragravity waves or surf beat. Infragravity waves propagate in horizontal direction with a phase velocity approximately given by $\sqrt{gh}$, where g is gravity acceleration and h is water depth. Slower velocities at shallower water depths tend to trap most of infragravity waves in shallow areas, where there are two types of freely propagating infragravity waves: edge wave and leaky wave. Edge waves are repeatedly refracted to be trapped in close proximity to the shore, whereas leaky waves can propagate to and from deep water.

[29] Oceanic infragravity waves are generated primarily by nonlinear interactions with higher-frequency gravity waves with dominant periods around 10 s [*Longuet-Higgins and Stewart*, 1962; *Munk*, 1949]. In shallow water of surf zone, these higher-frequency gravity waves steepen their fronts with increasing amplitudes. *Bowen and Guza* [1978] suggested that edge waves might become larger than leaky waves because they are trapped in shallow water (low-velocity region) where strong nonlinear forcing occurs.

[30] If the Earth is horizontally stratified, Rayleigh waves are decoupled with infragravity waves completely to first order. Some coupling mechanisms of infragravity waves with Rayleigh waves are required including those through seafloor topography. Topographic effect is expected to be significant near coastal areas including sea shelves where most of infragravity waves are trapped. Nonlinear wave-wave interactions of infragravity waves, if significant, are also expected in shallow sea.

[31] To examine the shallow sea contribution we make the following test. We distribute effective pressure sources homogeneously (1) over the whole sea surface, or on the seashore shallower than (2) 2000 m, (3) 1000 m or (4) 500 m. In each of these five cases, we expand the given source distribution by spherical harmonics and calculate the synthetic cross spectra between all the station pairs. The resultant cross spectra are inverted to recover the source distribution. We then plot the power of the recovered source distribution as a function of angular order l in Figure 10, where the power of each angular order is normalized by the

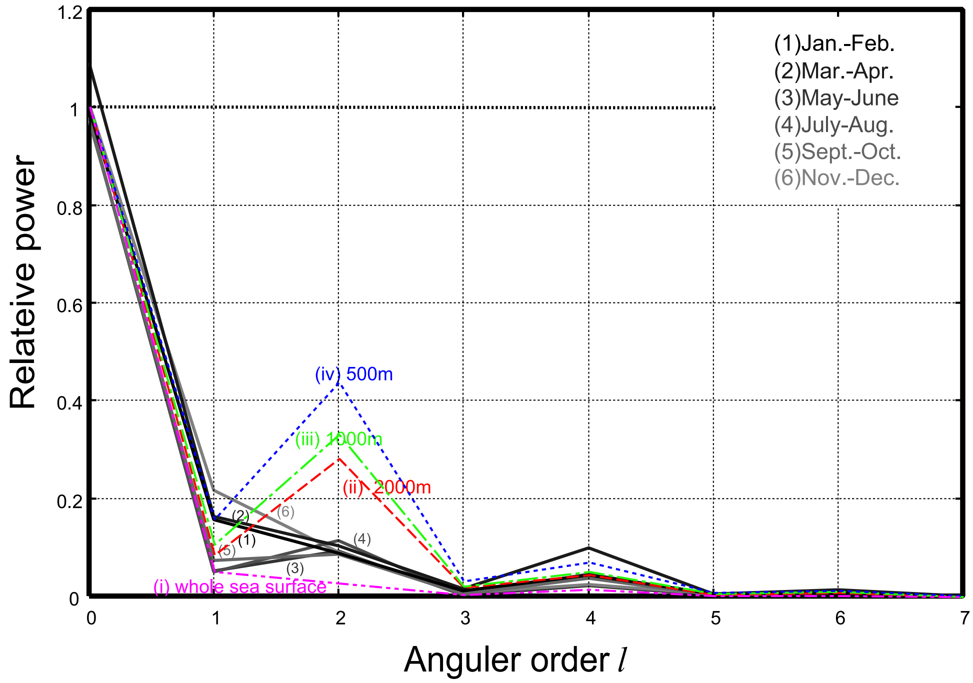

Figure 10. Power distribution of relative effective pressure structure ($\Sigma_m c_{lm}^2/4\pi$) for every 2 months of a year. Also plotted are the power distributions of the structures inverted from the synthetic data for homogeneously distributed sources on (line i) the whole sea surface and on the seashore shallower than (line ii) 2000, (line iii) 1000 and (line iv) 500 m. The power of each component is normalized by that of the 0'th component. The 3, 5, and 7 degree components are poorly resolved in part because of intrinsic difficulty of retrieving odd degree components and in part because of damping of our solution.

0'th power. Because of the damping applied in the inversion scheme, the 3, 5 and 7 degree components were poorly recovered, suggesting that this is also the case for the real data. It is obvious from Figure 10 that limitation of the source area to shallow seas makes the 2'nd degree contribution relative to the 0'th degree too large. A homogeneous distribution of excitation sources on the whole sea surface underestimates the observed relative power of the 2'nd degree component but it is still a better approximation than the shallow sea approximation.

[32] Atmospheric excitation mechanism can explain most of the observed statistical features [*Nishida and Kobayashi*, 1999], the annual variation of excited amplitudes [*Nishida et al.*, 2000], the observed acoustic resonance between the solid Earth and the atmosphere [*Nishida et al.*, 2000] and the observed amplitudes of the background free oscillations [*Fukao et al.*, 2002]. Atmospheric excitation mechanism can also explain the dominance of the 0'th degree source distribution, as revealed by the present study. Stronger excitations in oceanic areas may indicate stronger atmospheric disturbances there than on continents, although they alone may indicate more directly the presence of unknown excitation sources within oceans.

7. Conclusions

[33] We developed an inversion method for estimating the spatial distribution of excitation sources of Earth's background free oscillations from the cross spectra between pairs of stations. The method was applied to the real data from 54 stations over the world for 13 years. The results are given in every 2 months of a year. We confirmed a clear temporal variation of the spatial patterns. During the period from November to April the degree 1 pattern with its maximum intensity in the northern Pacific is dominant. In the period from May to August the excitation sources are located on the eastern and western Pacific rims through the Indian Ocean. The interval from September to October is a transitional stage between the above two periods. Through the year the excitation sources are broadly located on oceans. Sources on continents are weak. This temporal variation of the spatial pattern is qualitatively consistent with that of *Rhie and Romanowicz* [2004]. The spectral power distribution of the estimated spatial structure is so dominated in the 0'th degree that the excitation sources must spread over the almost whole sea surface. This feature suggests that ocean infragravity waves alone cannot explain observed spatial structure. Although they alone may indicate the presence of unknown excitation sources within oceans, atmospheric disturbances stronger on oceans than in continents can explain as well the observed spatial pattern of the excitation sources.

[34] **Acknowledgments.** We are grateful to a number of people who have been associated with the Black Forest Observatory, China Digital Seismic Network, Berkeley Geysers Network, TERASCOPE, Geoscope and IRIS since their inceptions for maintaining the networks and making the data readily available. We wish to thank N. Kobayashi for valuable discussions on this study. We also thank two reviewers (J. Ritsema and R. Widmer-Schnidrig) and the Associate Editor (J. Mutter) for many constructive comments.

References

Bowen, A., and R. Guza (1978), Edge waves and surf beat, *J. Geophys. Res.*, *83*, 1913–1920.

Dahlen, F., and J. Tromp (1998), *Theoretical Global Seismology*, 1025 pp., Princeton Univ. Press, Princeton, N. J.

Ekström, G. (2001), Time domain analysis of Earth's long-period background seismic radiation, *J. Geophys. Res.*, *106*, 26,483–26,494.

Fukao, Y., K. Nishida, N. Suda, K. Nawa, and N. Kobayashi (2002), A theory of the Earth's background free oscillations, *J. Geophys. Res.*, *107*(B9), 2206, doi:10.1029/2001JB000153.

IRIS, Inc. (1994), *Federation of Digital Broad-Band Seismograph Networks Station Book*, Washington, D. C.

Kobayashi, N., and K. Nishida (1998), Continuous excitation of planetary free oscillations by atmospheric disturbances, *Nature*, *395*, 357–360.

Larson, E. W. F., and G. Ekström (2001), Global models of surface wave group velocity, *Pure Appl. Geophys.*, *158*(8), 1377–1400.

Longuet-Higgins, M. S., and R. W. Stewart (1962), Radiation stress and mass transport in gravity waves, with application to surf-beats, *J. Fluid Mech.*, *13*, 481–504.

Munk, W. (1949), Surf beats, *Eos Trans. AGU*, *30*, 849–854.

Nawa, K., N. Suda, Y. Fukao, T. Sato, Y. Aoyama, and K. Shibuya (1998), Incessant excitation of the Earth's free oscillations, *Earth Planet. Space*, *50*, 3–8.

Nishida, K., and N. Kobayashi (1999), Statistical features of Earth's continuous free oscillations, *J. Geophys. Res.*, *104*, 28,741–28,750.

Nishida, K., N. Kobayashi, and Y. Fukao (2000), Resonant oscillations between the solid earth and the atmosphere, *Science*, *87*, 2244–2246.

Nishida, K., N. Kobayashi, and Y. Fukao (2002), Origin of Earth's ground noise from 2 to 20 mHz, *Geophys. Res. Lett.*, *29*(10), 1413, doi:10.1029/2001GL013862.

Rhie, A., and B. Romanowicz (2004), Excitations of the earth's incessant free oscillation by atmosphere/ocean/solid Earth coupling, *Nature*, *431*, 552–556.

Rost, S., and C. Thomas (2002), Array seismology: Methods and applications, *Rev. Geophys.*, *40*(3), 1008, doi:10.1029/2000RG000100.

Shapiro, N., M. Campillo, L. Stehly, and M. Ritzwoller (2005), High resolution surface wave tomography from ambient seismic noise, *Science*, *307*, 1615–1618.

Snieder, R. (2004), Extracting the Green's function from the correlation of coda waves: A derivation based on stationary phase, *Phys. Rev. E*, *69*(4), 046610, doi:10.1103/PhysRevE.69.046610.

Suda, N., K. Nawa, and Y. Fukao (1998), Earth's background free oscillations, *Science*, *279*, 2089–2091.

Tanimoto, T. (1998), State of stress within a bending spherical shell and its implications for subducting lithosphere, *Geophys. J. Int.*, *134*, 199–206.

Tanimoto, T. (1999), Excitation of normal modes by atmospheric turbulence: Source of long period seismic noise, *Geophys. J. Int.*, *136*, 395–402.

Tanimoto, T. (2005), The oceanic excitation hypothesis for the continuous oscillations of the Earth, *Geophys. J. Int.*, *160*, 276–288.

Watada, S. (1995), Part i: Near-source acoustic coupling between the atmosphere and the solid earth during volcanic eruptions, Ph.D. thesis, Calif. Inst. of Technol., Pasadena.

Watada, S., and G. Masters (2001), Oceanic excitation of the continuous oscillation of the Earth, *Eos Trans. AGU*, *82*(47), Abstract S32A-0620.

Y. Fukao, Japan Agency for Marine-Earth Science and Technology, 2-15 Natsushima-Cho, Yokosuka-city, Kanagawa 237-0061, Japan. (fukao@jamstec.go.jp)

K. Nishida, Earthquake Research Institute, University of Tokyo, 1-1-1, Yayoi, Bunkyo-ku, Tokyo 113, Japan. (knishida@eri.u-tokyo.ac.jp)